Title
Thermally-induced miniaturization for micro- and nanofabrication: progress and updates.

Journal
Lab on a Chip, 14(18)

Authors
Lin, Sophia
Lee, Eugene
Nguyen, Nancy
et al.

Publication Date
2014-09-21

DOI
10.1039/c4lc00528g

Peer reviewed

HHS Public Access

Author manuscript

Lab Chip. Author manuscript; available in PMC 2022 May 03.

Published in final edited form as:

Lab Chip. 2014 September 21; 14(18): 3475–3488. doi:10.1039/c4lc00528g.

Thermally-induced miniaturization for micro- and nanofabrication: progress and updates

Sophia Lin[a], **Eugene K. Lee**[b], **Nancy Nguyen**[b], **Michelle Khine**[a,b]

[a]Department of Chemical Engineering and Materials Science, University of California, Irvine, Irvine CA 92627, USA.

[b]Department of Biomedical Engineering, University of California, Irvine, Irvine CA 92627, USA.

Abstract

The field of micro- and nanofabrication has developed extensively in the past several decades with rising interest in alternative fabrication techniques. Growth of these areas has been driven by needs that remain unaddressed by traditional lithographical methods: inexpensive, upscalable, biocompatible, and easily integrated into complete lab-on-a-chip (LOC) systems. Shape memory polymers (SMPs) have been explored as an alternative substrate. This review first focuses on structure fabrication at the micron and nanoscale using specifically heat-shrinkable SMPs and highlights the innovative improvements to this technology in the past several years. The second part of the review illustrates demonstrated applications of these micro- and nanostructures fabricated from heat-shrinkable SMP films. The review concludes with a discussion about future prospects of heat-shrinkable SMP structures for integration into LOC systems.

Graphical Abstract

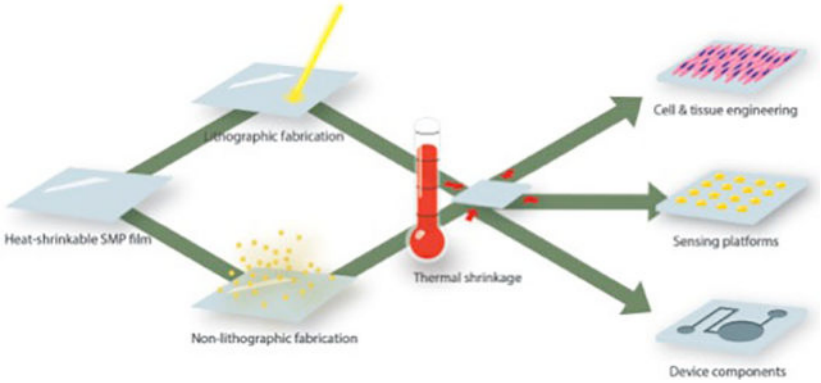

This paper reviews progress in micro- and nanofabrication achieved using heat-shrinkable shape memory polymers (SMPs) and the demonstrated applications of the resulting technologies.

mkhine@uci.edu .

1. Introduction

Micro- and nanostructures have a wide range of applications in the electrical, mechanical, biological, and optical fields. As such, much work has been done to fabricate structures at these length scales. Traditional fabrication methods for structures at the micro- and nanometer scales use techniques inherited from the semiconductor industry. While successful, these methods, such as photolithography, thin film deposition, and etching, face drawbacks such as the need for expensive cleanroom facilities and the use of harsh, environmentally damaging reagents. Resulting structures can also suffer from limited resolution and planarity. These properties hinder progress towards rapid and inexpensive scale up that many emerging applications, particularly lab-on-a-chip (LOC), necessitate.

To address these issues, unconventional methods for micro- and nanofabrication have been devised and have been reviewed extensively.[1–5] These methods, for example molding, embossing, and self-assembly, have allowed for fabrication of structures with complex geometries and improved resolution over large areas at increased speeds.[5–7] One relatively new area of exploration involves the use of shape memory polymers (SMP) for micro- and nanofabrication.

SMPs are stimuli responsive materials that result in mechanical action when triggered by an external stimulus.[8] An SMP is composed of randomly coiled polymer chains that can be deformed and fixed. Application of an external stimulus results in shape recovery of the SMP. External stimuli can be broadly categorized into photo,[9–13] chemical,[14, 15] or thermal stimuli.[16] Photo-stimuli involve using specific wavelengths of light to excite the photo-reactive molecules in the SMP. The molecular changes of the photo-reactive groups are then manifested as macroscopic changes of the SMP. Chemical stimuli, which can include water, pH, and various solvents, work by decreasing the glass transition temperature, T_g, of the SMP to initiate shape recovery. On the other hand, thermal stimuli involve triggering the SMP by raising the SMP above its characteristic T_g. This is accomplished by either directly heating the SMP or indirectly heating the SMP using electromagnetic fields or photo-illumination.

These polymeric smart materials are inexpensive, have convenient processing and fabrication techniques, as well as programmable and controllable behavior. These properties are advantageous for the translation of laboratory techniques to scalable and manufacturable technologies. Many literature reviews covering SMPs, its progress, applications, and current challenges have been published and will not be the focus of this review.[8, 16–23] Instead, we aim to spotlight SMP materials that undergo heat-induced miniaturization for LOC applications.

Heat-shrinkable SMPs, which were first reported to be used in the packaging industry in the 1960s,[24, 25,28,29] have recently been applied towards a micro- and nanofabrication platforms. These heat-shrinkable materials, comprised of cross-linked polymer chains, such as polyethylene,[24] poly(ethylene terephthalate),[26] and polystyrene,[27] are extruded, molded, and cross-linked. The semicrystalline materials are then heated, stretched, and then cooled to “freeze in” the oriented polymer structure.[28–31] Release of the stored

elastic stress and recovery to original shape occurs when heat is applied. Studies have characterized the polymers' thermal behavior and shrink mechanism,[31–38] as well as their performance as packaging materials.[25, 39–41] Presently, SMPs lend themselves to innovative processing techniques compatible with traditional lithographic methods. This allows the ability to substitute less-expensive approaches yet achieve improved resolution and/or create otherwise difficult to fabricate architectures (such as multi-scale features). Therefore shrink-based processing is not intended to necessarily be a complete replacement of traditional fabrication technologies, but rather as a synergistic and compatible technique that can enhance resolution and expand design capabilities. Here, we specifically review heat-retracting SMPs' use in micro- and nanofabrication and the current applications of these resulting features with an emphasis on their utility in LOC technologies. Fabrication techniques and current applications are discussed (Fig. 1). This review will also discuss current limitations of this technology and conclude with future outlooks.

2. Micro- and nanofabrication using shrink technology: structure fabrication and improved resolution

We first present different approaches that have been employed to fabricate structures at the micro- and nanoscale using pre-stressed heat-shrinkable SMP materials. These methods can be broadly categorized into lithographic and non-lithographic methods. We define lithographic as using surface patterning methods to introduce structures on the SMP material, and non-lithographic as leveraging the inherent surface instability of the SMP material for structure fabrication.

2.1 Structure fabrication and improved resolution

Lithographic methods for patterned micro- and nanostructures—Micro- and nanofabrication using heat-shrinkable SMP take advantage of the elastic memory of the polymer material. Relaxation of the heat-shrinkable pre-stressed SMP by heating above the T_g leads to shrinkage of the SMP in the plane of the film. This process results in the size reduction of surface patterned features, as first demonstrated by the Whitesides group.[42–44] By defining structural regions with a physical mask on the polystyrene (PS) surface, etching the surface with O_2 plasma to physically remove the material, and applying heat at T = 110 °C, authors were able to improve the aspect ratio of the etched trench by a factor of ~100-fold (shrinkage increased the feature aspect ratio from ~0.1 to ~9.7). The molds created using the shrinkable PS polymer were also used for replica molding, resulting in microstructures of other materials such as carbon, gold, and sol-gel silica.[43, 44] Hidber *et al.* also showed that shrinkage of a patterned seed layer on prestressed PS allowed for formation of smaller plated copper features whose sizes corresponded with the shrinkage amount expected from polymer processing.[42] Lee *et al.* created microstructured pillars by using the heat-shrinkable polyvinylchloride (PVC) and polyolefin (PO) film as a template.[45] By laser machining holes into the film, shrinking, and then filling with epoxy, authors were able to form arrays of microstructured pillars with diameters reduced by a factor of 5. Embossing (a well-established low-cost alternative fabrication method that involves imprinting patterns at controlled temperatures and pressures) can be combined with the shrink film technology to create high aspect ratio structures with reduced feature size. Zhu *et al.* showed that physical

removal of hot embossed features on PS film through polishing results in the inverse of the molded structures when shrunk, circumventing the problem of material reflow due to the shape memory effect. [46] In this study, micron-sized pillars and posts were created. However, one can imagine that this approach can be adopted by nanoimprint lithography to create even smaller features. Integration of embossing techniques with the shrink technology offers a fabrication of high density arrays at faster speeds—lending itself a powerful method towards manufacturability.

These studies demonstrate a relatively rapid and inexpensive method to fabricate multi-dimensional structures down to the nano-scale level. Fabricated structures also have dramatically increased aspect ratio compared to the pre-shrunk structures. However, sizes of the fabricated features are limited by the degree of shrinkage achievable by the pre-stressed SMP, a property dependent on the polymer's extrusion process. The smallest structures reported in the previously discussed studies were ~1.4 μm x 1.7 μm.[43, 44] Structures in the nanometric regime (generally agreed as having features < 100 nm) are achievable using conventional photolithography and more recently, imprint lithography. Efforts to improve structure resolution to reach nanometric levels using heat-shrinkable technology persist. Progress within the past several years has yielded several innovative methods to obtain structures with improved resolution using heat-shrinkable films.

Our group has improved upon the shrink technology and has shown that we are able to fabricate even smaller structures with improved aspect ratio by using polyolefin (PO) shrink wrap film. [47] This polymer can shrink reproducibly up to 95% in area, allowing for fabrication of even smaller features compared to that made on PS. While polymer shrinkage is limited by the draw ratio (the amount of inputted pre-stress), Cui and coworkers have overcome this limitation and improved feature resolution obtained using the shrink technology by incorporation of hot-embossing techniques (Fig. 2).[48] By embossing sharp-tipped nickel (Ni) molds at high pressures (35 – 55 kN) into PO film, shrinking, and then using the resulting substrate as a shadow mask, Zhang *et al.* were able to pattern lines of different widths, with the smallest line being 21 nm wide. This was vastly thinner than the expected theoretical line width of ~46 μm (955D PO film experiences a 77% reduction lengthwise) as the original patterned lines were 200 μm wide. The results were attributed to the local deformation of the PO film from embossing at high pressures. This represents a novel method to pattern features at the nanometer scale resolution.

Non-lithographic methods for micro- and nanostructure fabrication—Micro- and nanoscale features can also be derived from the surface wrinkling phenomenon. This non-lithographic method for structure fabrication using the heat-shrinkable SMP takes advantage of mechanical instabilities that exist between the compliant SMP and a skin layer. Surface wrinkling has been an active area of research as wrinkles have been harnessed for a wide variety of applications such as sensing, optical gratings, electronic devices, and adhesion.[49–52] Excellent reviews exist that discuss the mechanics and dominating forces behind the surface wrinkling phenomenon and existing applications.[53–55] Briefly, surface wrinkling arises from the stiffness mismatch between layered dissimilar materials. For example, an elastomeric material such as polydimethylsiloxane (PDMS) (which easily compresses and expands) can be used as a substrate for a stiff skin layer. Release of

the elastomer's elastic stress causes the skin layer to buckle and fold, forming wrinkled structures.[56] The wrinkle amplitudes and wavelengths have been shown to be dependent on the thickness of the skin layer and the films' elastic properties.[57, 58] While PDMS has become a staple of the microfluidics community, its material properties present drawbacks such as swelling, leaching, and limited deformation.[59, 60] The heat-shrinkable thermoplastic film represents an attractive alternative as a platform for wrinkle formation because film processing is compatible with roll-to-roll manufacturing, allowing for potential scale-up of fabricated technologies.

We first reported the ability to create micro- to nanoscale wrinkles using the heat-shrinkable SMP film.[61] To do so, a thin layer of gold was deposited onto pre-stressed PS. The substrate was shrunk by heating to the PS's T_g. Retraction of the PS film caused the stiff non-shrinkable gold layer to buckle and fold, thus creating multiscale wrinkles. Both uniaxial and biaxial wrinkles were formed by simply changing the boundary conditions (Fig. 3). Control of wrinkle dimension was done through varying the thickness of the gold skin layer. Using the heat shrinkable PS, we were able to create wrinkles with feature sizes down to 200 nm and 300 nm for the uniaxial and biaxial wrinkles, respectively. Huntington *et al.* also leveraged the self-retracting properties of the heat-shrinkable films and showed that reduction of the skin layer's elastic modulus generated even smaller nanoscale wrinkles (250 to 50 nm). [62] Skin layers on the PS substrate were established via reactive ion etching (RIE) with the gases SF_6, CF_4, CHF_3, or Ar. Unique to Ar gas, researchers were able to directly correlate wrinkle wavelength and skin thickness. This potentially allows for direct control over resulting wavelength size for specific applications.

Heat-shrinkable polymer films represent simple, versatile, and cost effective platforms for patterned micro- to nanoscale sized features with different orientations and size distributions. It is of interest to generate different patterns using the heat-shrinkable polymer due to the wide range of applications these patterns can address. Alternate wrinkle patterns such as herringbones, [63, 64] labyrinths, stripes, rings, and radial shapes [65] have been created on elastomeric substrates such as PDMS and self-strained SMP. These patterns are accomplished by varying the applied pre-strains and surface conditions. Researchers have thus far only reported uniaxial and biaxial wrinkle formation on the pre-stressed heat-shrinkable SMP films. Structure variability on the heat-shrinkable SMP is an ongoing area of interest as this will allow for better control and flexibility for desired applications.

Structure tunability—Heat-shrinkable SMP films allow for a high degree of flexibility for structure fabrication. The amount of shrinkage of patterned features and array densities can be easily controlled by the temperature applied to the SMP substrate. Microarray density can also be controlled via shrinkage degree. Lee *et al.* combined soft lithography with the heat shrink technology to create nanoscale photoresist patterns of different array densities based off a single master mold. [66] A PDMS stamp was used to transfer the photoresist patterns onto the PS thermoplastic. Heat shrinkage at different temperatures (above the T_g) resulted in arrays with pitches that were smaller than the original master mold. Additionally, by bringing the patterned SMP to a temperature above the T_g and uniformly stretching the substrate, the pitch size was increased. These substrates could then be molded with PDMS to create subsequent masters for feature transfer onto functional materials. This work

demonstrated a simple yet powerful method for rapid prototyping using a single master mold.

Surface wrinkle sizes can be tuned to specific wavelengths by changing the thickness of the elastic skin layer, the material properties of the film and substrate, and the overall shrinking strain produced. These properties can be understood by examining the wrinkling equations, and theoretical predictions have been verified as mentioned above.[61, 67] Fu *et al.* verified theoretical predictions by showing that changing the deposited gold layer's thickness from 10 nm to 50 nm caused a shift in resulting wavelengths.[61] Huntington *et al.* showed a direct correlation between wrinkle wavelength and thickness of the stiff skin layer produced by CHF_3 RIE (Fig. 4).[62] Consideration of each factor in the wrinkling equation is necessary for control over resulting wrinkle wavelength.

Beyond planar structures—Up to now in this review, the structures discussed have resided on planar surfaces. This coincides with traditional lithographic methods as fabricated structures are limited to planar substrates. Several groups have leveraged the self-retracting property of the SMP films for non-planar structure fabrication. The heat-shrinkable SMP reflows when brought above the T_g and this property allowed for the formation of rounded channels. [68] Luo and coworkers took advantage of the reflow properties of the heat-shrinkable SMP and introduced a pressing step into their process. By patterning onto the pressed PS, and then relieving the secondary strain, they were able to generate surface patterns ranging from Ag dots, lines, and serpentine traces on the PS sidewalls.[69] Luo and coworkers further developed this technique and incorporated the sidewall patterns onto PS microchannels (Fig. 5).[70] This simple yet innovative way for structure fabrication onto nonplanar surfaces has the potential to expand applications of heat-shrinkable SMP-derived structures.

The reflow property of heat-shrinkable SMP materials has also been leveraged for the formation of 3-dimensional structures. Liu *et al.* showed that the PS film could self-fold due to localized light absorption.[71] By defining regions of black ink onto the planar surface and heating with an IR heat lamp, they were able to introduce hinges where the SMP would fold. Folding degree and speed could be controlled by the line width and light exposure time. Much remains to be explored for self-folding heat-shrinkable SMP materials as effects such as variable light intensity, wavelength, and hinge material (to name a few) can be changed. Heat-shrinkable SMP materials represent highly flexible substrates that allow for structure fabrication beyond planar surfaces.

3 Applications of micro and nanostructures fabricated using heat-shrinkable SMP films

Structures derived from heat-shrinkable SMP films have been applied to various avenues because of the unique properties that arise from thermoplastic polymer shrinkage. Structure fabrication is inexpensive and fast, and resulting structures are easily integrated into LOC technologies. We present some applications of these micro- and nanostructures that have been reported within the past several years. Applications can be broadly categorized for cell and tissue engineering, sensing and detection, and microfluidic sample processing.

3.1 Cell & tissue engineering

Tunable structures formed from heat-shrinkable SMP materials have directly translated towards two types of cell and tissue engineering applications, nanobiomimicry and cell culturing platforms. Heat-shrinkable SMP materials can be used to generate biomimetic structures that guide cell alignment. The shrink technology also allows for facile production of microwells, allowing for controllable formation of cell aggregates with designated sizes. Below we will discuss the development and importance of these tissue engineering applications.

Biomimetic material for cell alignment—Tissue regeneration and *in vitro* organ models are core components of the tissue engineering field. Therefore it is critical that cells used in such systems have the same genotypic and phenotypic profile as their native counterparts. Both physical cues and chemical factors can influence cellular expression and function. In certain organ systems, the extracellular matrix (ECM) is composed of anisotropic fibrils that provide physical cues for cellular alignment. Specifically, within the cardiovascular system, the alignment of cardiomyocytes can have a profound impact on the behavior of the heart.[72] Grosberg *et al.* demonstrated that the alignment of cardiomyocytes alone can align sarcomere structures, produce stronger contractile forces, and generate anisotropic action potential.[73] Thus, the capability to recapitulate the anisotropic nature of the ECM can affect the efficacy of tissue regeneration methods and *in vitro* organ models.

Alignment of cardiomyocytes and cardiac-related cells—Luna *et al.* first demonstrated that heat-shrinkable SMP materials could be used to fabricate biomimetic materials with an anisotropic topography.[74] Gold-palladium was sputtered onto pre-stressed PS sheets and uniaxially-aligned heterogeneous wrinkles were generated by constraining the opposite sides of the film during shrinkage. Dependent on the thickness of the sputtered skin layer, wrinkles had length-scales ranging from 20 nm to 1 μm. The features of these PS sheets were transferred to PDMS substrates via soft lithography. Neonatal mouse cardiomyocytes and human embryonic stem cell (hESC)-derived cardiomyocytes were seeded onto the PDMS substrates. Immunostaining showed that cells seeded on the wrinkled substrates displayed greater alignment (preference towards an axis) than those cultured on a flat surface. Additionally, the hESC-derived cardiomyocytes exhibited an organized sarcomeric banding pattern similar to those found in the native myocardium

Chen *et al.* devised another method to create biomimetic materials for cellular alignment.[75] Instead of using a metal layer to induce wrinkle formation onto heat-shrinkable polyethylene (PE), O_2 plasma treatment was used to form the stiff skin layer. Similarly the treated film is constrained on opposing sides and shrunk to generate anisotropic features. Using voltage sensitive dye and point stimulation, Chen *et al.* showed that hESC-derived cardiomyocytes on wrinkled substrates had an action potential that was faster in longitudinal conduction velocity than the control (2.13 + 0.11 cm s^{-1} and 1.82 $\pm$ 0.20 cm s^{-1} respectively). This further supports that the anisotropic nature of the ECM plays an important role on the behavior of native cardiomyocytes.

Both fabrication methods provide a rapid, effective, and low-cost alternative to create materials with biomimetic surfaces without heavy tooling. Unlike features derived from the abrasion and electrospinning techniques, SMP generated features span multi length-scales, which are similar to the size ranges of fibrils found within the ECM.[76–80] Techniques such as colloidal lithography have been used to create nanotopographical features; however, such techniques have only been shown to produce randomly ordered and oriented features.[81] SMP-based methods allow the tailoring of wrinkle size and orientation.

The biomimetic materials fabricated from SMP-based methods have been implemented in various cardiac-related projects. Wang *et al.* demonstrated that monolayers of hESC-derived ventricular cardiomyocytes aligned on the biomimetic surfaces were less susceptible to spontaneous and inducible arrhythmias (57% for control vs. 17–23% for aligned cells).[82] This effect was attributed to anisotropy-induced electrical stability and not genotypic changes to the cells, suggesting that the ventricular cardiomyocytes grown on the biomimetic substrate would be a more accurate model for arrhythmogenicity screening of pharmacological and genetic factors. Turner *et al.* integrated these biomimetic substrates into proposed packaging and delivery systems of cardiac cells for tissue regeneration purposes.[83] A novel approach to lift off cells aligned on the biomimetic substrate was performed by grafting thermosensitive poly(N-isoproylacrylamide) (p-NIPAAM) onto the substrate surface prior to seeding. While functional cardiac tissue for implantation was not achieved, the study combined various cell tissue engineering techniques, such as the biomimetic substrate and p-NIPAAM surface graft, into tools that bring the tissue engineering field one step closer to generating implantable tissue.

Chen *et al.* paired hESC-derived cardiomyocytes aligned on biomimetic substrates with optical flow techniques based on bright-field images to create a drug-screening platform for cardiotoxicity (Fig. 6).[84] To demonstrate the efficacy of the platform, two drugs, E-4031 and isoprenaline, were examined. Cardiomyocytes aligned on the biomimetic substrate responded to a lower dosage of E-4031 compared to the traditional IC_{50} assay. The enhanced responses suggest that the integration of aligned cardiomyocytes into drug screening platforms can create more efficacious assays.

Other tissue engineering projects—Cell alignment on the biomimetic surface is not limited to cardiomyocytes and associated cardiac derivatives. Other cell types such as mouse embryonic fibroblasts, aortic smooth muscle cells, hESC, mouse ESC-derived endothelial cells, and mouse myoblasts have been shown to align on the wrinkled surfaces. [74, 75, 82–86] Hatano *et al.* studied the topographical effects of mouse ESC-derived endothelial cells by seeding the cells on numerous surfaces, including two biomimetic surfaces with uniaxial wrinkles of different length-scales.[85] Using fluorescence-activated cell sorting (FACS), they characterized the ESC-derived endothelial cells as a micro-vessel subphenotype and found they best aligned on the nano-scale wrinkled surfaces. The length-scale of the fabricated nanowrinkles is consistent with the fiber size found in the micro-vessel subphenotype's basement membrane where endothelial cells are located.

Greco *et al.* aligned C2C12 mouse myoblasts onto a biomimetic substrate fabricated in a method similar to that of Luna *et al.*[86] They spun a conducting polymer, poly(3,4-

ethylenedioxythiophene):poly(styrene sulfonate) (PEDOT:PSS), onto the surface of a PS film. The effects of the topographical features of the biomimetic surfaces on C2C12 adhesion and proliferation were consistent with previous studies that used substrates with similar length scales. Furthermore, wrinkled features were shown to guide cell differentiation as aligned C2C12 cells differentiated into multinucleated and elongated myotubes. More importantly, the demonstrated ability to pattern on the PEDOT:PSS layer through local overoxidation suggests the potential of a quick and low cost method to create biocompatible electrodes for cell tissue engineering purposes.

3.2 Cell microarrays

The introduction of induced pluripotent stem cells and advancement in stem cell technology have resulted in many new and established differentiation protocols that require formation of embryoid bodies (EBs) or stem cell aggregates. The three most common techniques for EB formation are suspension culture in low adhesion dishes, culture in methyl cellulose, and culture in hanging drops. Disadvantages of these methods include lack of control and reproducibility, the need for intensive manual labor, and difficulty for scale-up.[87]

Cell microarray for embryoid body formation—To address the limitations of current EB culture methods, Chen *et al.* developed a simple and rapid culturing platform using the heat-shrinkable SMP material. Micro-well patterns were first printed onto the pre-stressed PS sheet (a method first established by Grimes *et al.*) using a laser jet printer. [88, 89] The printed film was thermally annealed, resulting in raised circular hemispheres, and then molded against PDMS to create PDMS micro-well arrays. Cells of a pre-determined concentration were loaded into the micro-wells via centrifugation and EB maintenance was carried out in a normal petri dish. This system allowed for a more efficient medium exchange process. Unlike the 96-well low adhesion plates, the medium for all wells could be replaced at once. By pipetting the medium in and out from the side of the substrate in a slow and cautious manner, the cells would not be disturbed and move out of the micro-wells during the exchange.

Nguyen *et al.* expanded upon this platform and evaluated the efficacy of these micro-wells.[90] Instead of a rectangular array of micro-wells, a honeycomb configuration was used to maximize the number of EBs formed. To demonstrate the controllability of EB size, three types of micro-wells with different dimensions (diameter and depth) were fabricated and inserted into a standard 24-well plate. With an improved loading process, centrifugation was no longer required as a solution of predetermined cell concentration could be directly pipetted onto the honeycomb patterns. It was shown that the EB size was linearly correlated to the well size. Therefore, a way to achieve desired aggregate size could be controlled by either micro-well size or cell loading density. This method was able to produce EBs of similar size to those formed with the hanging drop method (200 μm in diameter) but holds the potential for scale up.

Microarray for Single Cell—Lew *et al.* used the heat-shrinkable SMP film to create single-cell culturing platforms by making microwells with diameter sizes of 20, 40 and 60 μm.[91] Pre-stressed PO (which experiences greater shrinkage than PS) was used. A

shadow mask was formed by laser cutting an array of holes into PO tape. The PO tape was then adhered to the pre-stressed PO sheet and O_2 plasma etched to create shallow wells. The PO film was thermally annealed to produce deep wells directly in the plastic film. This fabrication technique avoids the use of PDMS, which has been shown to alter the biochemical environment over time. To demonstrate the effectiveness of the platform, both fluorescent beads and calcein AM-stained single hESC were loaded separately into the micro-wells. This low-cost and easily fabricated platform can provide researchers an easily accessible method to conduct longitudinal single-cell studies along with cell-cell interactions or cell-substrate interactions.

3.3 Detection

Protein, small molecule, and analyte detection is particularly important in the area of disease diagnostics as early detection has been correlated with better prognosis. Hierarchical structures produced on the heat-shrinkable SMP films have been applied towards chemical and biological sensing and are easily integrated into LOC devices. The following sections illustrate the use of these structures for sensing applications, namely optical, electrochemical, and plasmonic sensing.

Optical sensing—Optical readout methods based on colorimetric, luminescent, and fluorescent signals have been largely used in detection assays because of established instrumentation and methods, particularly in the field of biological sciences. These assay techniques not only are compatible with structures made on the heat-shrinkable SMP films and but also show improved sensitivity based off inherent properties of the shrink technology.

Le Goff *et al.* patterned DNA-hydrogel microarrays onto a PS surface and showed that shrinkage of the DNA microarray resulted in submicron 3D spots.[92] Enhanced detection sensitivity on the shrunk hydrogel over the flat polystyrene surface was attributed to increased surface area for oligonucleotide immobilization. Both colorimetric and chemiluminescent assays were shown to have improved detection capabilities on the DNA hydrogel, which also provided a hydrophilic environment for oligonucleotide immobilization. Shrinkage of the SMP film resulted in microarrays of increased surface area, suggesting the potential for improved probe density and subsequently increased signal. In the chemiluminescent assays, Le Goff *et al.* quantified the effects of the shrunk microarray on the efficiency of oligonucleotide immobilization by comparing signals obtained from the microdots to those from direct oligonucleotide spotting. At the lower target concentrations, the signals from the microarrays achieved as high as a 2.0 fold increase in intensity values.

Pegan *et al.* developed high surface area electrodes using PO shrink film and showed improved sensing capabilities on the shrunk Au electrodes over the thin film Au electrodes (Fig. 7).[93] The Au electrodes were used for electrochemiluniscent (ECL) sensing of 2-(dibutylamino)-ethanol (DBAE). The limit of detection (LOD) with the shrunk electrodes (1.7 μM) was more than two times lower than the reported values in similar paper-based ECL methods. The enhanced ECL sensing was attributed to the increased surface area of the

wrinkled Au electrode. The shrunk electrodes had a significant increase in electrochemically active surface areas (>600%) when compared to non-shrunk, planar electrodes. Shrinkage not only increased the surface area available for sensing applications, but also reduced the discontinuities between the deposited Au, lending the Au electrodes conductive behaviors similar to that of bulk materials.

Structures fabricated on the heat-shrinkable SMP film have also been incorporated into fluorescence-based sensing platforms. Multi-scale silica (SiO_2) structures were shown to enhance the fluorescence signal of bound fluorescently labelled proteins.[94] Upon shrinking the patterned PO film, bound biomolecules were brought closer together. Formation of rough, light-scattering SiO_2 structures constrained the linked biomolecules, subsequently inducing changes in biomolecules' photophysical properties. These factors contributed to the far-field fluorescence signal enhancement and allowed for increased sensitivity and lower LOD (11 ng mL^{-1} on the SiO_2 structures compared to 0.26 μg mL^{-1} the flat, planar control).

Electrochemical Sensing—Electrochemical sensing boasts high sensitivity and selectivity as well as provides quantitative output for detection of chemical species. Micro- and nanowrinkled palladium (Pd) structures formed on the PS film were used for hydrogen sensing.[95] Hydrogen absorption onto the Pd surfaces results in changes in electrical resistance. Complex behavior observed on the wrinkled Pd surfaces towards were attributed the effects of hydrogen absorption on both bulk/continuous films (from shrinking) and discontinuous/nanogap films (from surface structuring and increased surface area). The competition of the two effects resulted in a switching response on the Pd wrinkled surfaces when approaching a critical concentration the authors deemed as the "activation threshold." It was shown that the activation threshold could be tailored by changing the Pd feature sizes.

In contrast to direct integration of the conductive surface onto the SMP film, lithographic patterning of the sensing surface can be performed using a SMP film-derived shadow mask. Zhang used embossed PO as a mask to pattern suspended graphene nanoribbons (GNRs).[96] The suspended GNRs were used as ion-sensitive field-effect transistors (ISFET). The GNRs responded to changes in pH characterized by a positive shift in the Dirac point when pH increased (range of pH 5 to pH 9 tested). In addition, the suspended GNRs demonstrated improved sensitivity for prostate-specific antigens (PSA) over unsuspended and larger GNRs with an improvement in the LOD by 100-fold.

Plasmon-based sensing—Plasmon-based surface sensing takes advantage of the interactions between plasmons and substrate surfaces for electric field enhancements. Nano-sized features allow for powerful enhancements based off localized surface plasmon resonance (LSPR) effects that are not observed in bulk materials. Numerous nanostructure-based sensors have been developed to capitalize on these effects. Ross *et al.* developed high-density nanoplasmonic antenna arrays on the PS film using nanosphere lithography.[97] Polymer shrinkage resulted in contraction of the patterned Au nanoprisms, creating sub-10 nm nanogaps. Reduced nanogaps allow for increased localized electromagnetic fields, thus improving substrate molecular sensitivity. The heat-shrinkable SMP film was also used by Urban *et al.* to overcome the limit of resolution of optical force printing and reduce the spacing between Au nanoparticles.[98] Using a combination of optical force printing

and nanoimprint lithography, Urban *et al.* created arrays of particle dimers, trimers, and tetramers with nanogap spacings of between 20 to 40 nm. Plasmonic coupling was observed and quantified by scattering spectroscopy.

Metallic structures formed using the shrink film have also been reported as a platform for plasmon-enhanced fluorescence sensing.[61, 99] Fu *et al.* showed that annealing the PS polymer film patterned with Ag and Au led to cracking of the bimetallic layer. The resulting sharp nanopetals and nanogaps provided regions of localized hotpots for enhanced electric field. Fluorescence emission enhancements of up to 4000-fold on the metallic structures lend these surfaces powerful sensing applications. Sharma *et al* also leveraged the shrinkage properties of the SMP film to create hybrid Ni/Au structures for metal enhanced fluorescence (MEF) phenomena, and demonstrated the ability to achieve single molecule detection.[100] Sharp composite structures created using the heat-shrinkable PO film resulted in enhanced fluorescence emission of fluorescently labelled protein by more than three orders of magnitude. The magnetoplasmonic structures represent an integrated technology that has potential to both captures and detect minute concentrations of molecules.

LSPR effects arise when incident light with appropriate energy excites the electrons at the metal nanostructure's surface. The local electric field enhancements at the nanostructure surface augments surface enhanced Raman scattering (SERS) effects, resulting in greatly enhanced scattered radiation. SERS performance of Au[101] and Ag/Au nanoporous thin films[102] were improved by annealing the thin film on a PS surface (Fig. 8). Thermal contraction resulted in the formation of 3D bimetallic nanostructures with increased SERS efficiency over the flat nanoporous film. Chen and coworkers showed that cracks and sharp tips formed at the wrinkle's edges serve as "hot spots" for improved SERS enhancements. Crack formation can be controlled by the thin film nanoporosity.[101] Shrinkage of the nanoporous metal films created hot spots that improve the SERS effects of nanoporous thin films. Single molecule detection of rhodamine 6G and adenosine were achieved at these ridges.[102]

Heat-shrinkable SMP films provide opportune substrates to create highly sensitive plasmon-based sensing surfaces. Typical technologies to produce the nanoscale-sized features necessary for plasmon coupling can be expensive and suffer from limited resolution. Shrinkage of appropriate material deposited on the SMP film can improve resolution of nanogaps as described[97, 98] and also fabricate "hot spot" regions.[51,63,101, 102] Factors such as changing the nanoporosity of the metal thin film, metal film thickness, material composite, and patterning allow for tunability of fabricated structures and plasmon frequencies. This yields the ability to detect of a wide range of molecules. Compared to surfaces fabricated with traditional lithographic methods, surfaces derived from the pre-stressed polymer experience heterogeneity and increased system disorder.

3.4 Device components

Miniaturization of device components is important for integration into LOC systems. Heat-shrinkable SMP films have been used to generate functional components for microfluidic devices. We review basic elements of microfluidic systems, such as channels and mixing zones. We also showcase other individualized features derived from the heat-shrinkable

SMP films, such as separation and purification traps, optical systems, and energy conversion platforms.

Microfluidic channels—Channels are basic components of microfluidic systems that transport samples throughout the device, allowing for on chip sample manipulation and analysis. Rounded microfluidic channels have been made via microelectromechanic systems (MEMS) processes. However, as mentioned, these methods require heavy tooling and do not lend themselves to easy scale-up. To address these issues, Grimes *et al.* leveraged the inherent shrink properties of pre-stressed PS film and demonstrated a non-photolithographic method to create channels.[89] Channels were printed onto PS film using a desktop laser jet printer, shrunk, and molded with PDMS. Shrinkage of the patterned PS film caused the ink to increase in height by over 500%. The raised ink features with increased aspect ratio were molded into deep and rounded PDMS channels. Microchannel functionality was demonstrated by using the resulting microdevice as a gradient generator and a platform for cell flow through. Channels with heights up to 80 μm and widths down to 60 μm were achieved with this method. This approach represented a novel, rapid, and low-cost method to create rounded channels, a property difficult to achieve with traditional fabrication methods.

Chen *et al.* created microfluidic chips directly using the heat-shrinkable SMP film.[68] Channels were made by engraving onto unshrunk PS film and shrinking. Thermal shrinkage of the engraved channels resulted in decreased channel width and increased channel depth. Channel dimensions were controlled by the applied pressure, tip shape, and scriber size. Stacking the PS sheets allowed for creation of 3D microfluidic devices and eliminated the need for PDMS. Taylor *et al.* further built upon this method to create microfluidic devices using the heat-shrinkable PO film (which experiences a higher shrink ratio than PS).[103] Channels were designed using a digital craft cutter, which allowed for channel uniformity as well as smooth surfaces and vertical side walls. Microchannel functionality was demonstrated via an integrated immunoassay. While resulting microchannel sizes are limited by the original lithographic printing method (in the discussed studies: the printer resolution, scribed thickness, and craft cutter resolution), they are achievable using many different patterning approaches.

Channels fabricated using the heat-shrinkable SMP film have been used for a variety of applications. Swaminathan and Cui created PDMS microfluidic channels using printed PS as the master mold (as established by Grimes *et al.*) and used these channels to identify specific peptide binding motifs to PDMS via phage display technology.[104] This technology has allowed for the development of bifunctional peptides for the binding of other materials to PDMS, such as streptavidin. Chakraborty *et al.* also leveraged the strain-recovery properties of the heat-shrinkable PS to create superhydrohobic channels.[105] Shallow channels were introduced onto the prestressed PS surface via masking and O_2 plasma etching. Ag microdots were deposited onto the etched surface and etched again with O_2 plasma. Thermal annealing of the PS substrate resulted in the formation of micro and nanostructures, rendering the channels superhydrophobic. This property could be used to reduce drag forces in microfluidic applications, increasing transport efficiency and device performance. The heat-shrinkable SMP film represents a platform to create high aspect ratio channels with reduced feature sizes important to integrated LOC systems. Improved

chemical compatibility, surface functionality, and optical clarity of the thermoplastic-derived microdevice represent increases in applications achievable by these systems.

Mixing & separation/purification—The ability to effectively micromix fluids on-chip is important for sample processing and analysis. Effective micromixing is often difficult to achieve and ingenious designs such as the “square-wave” mixer have been proposed to address mixing at the two-dimensional (2D) level. [106] However, long-length scales are still required to achieve passive diffusion.[107] Micromixing at the three-dimensional (3D) level has been difficult to achieve due to the complexity of the fabrication process itself. Heat-shrinkable SMP films have been used to fabricate components that lend themselves to effective mixing at the microscale. Long *et al.* created a 3D microvortex mixer using the heat-shrinkable SMP film and observed a 3.5-fold improvement of the mixing index (at Reynolds number 10) in the 3D microvortex mixer compared to the 2D square mixer. The mixing index was based off intensities of the outlet and inlet streams.[107] Jayadev *et al.* also used the heat-shrinkable SMP film to fabricate an open mixing platform.[108] An inexpensive superhydrophobic substrate for molecular assays was introduced by patterning a microarray of “sticky” spots and depositing droplets of test solution on the patterned spots. Fluid mixing was easily achieved without concern of depositing some of the test solution at the non-detection spots, due to the substrate’s superhydrophobicity.

Alternatively, the heat-shrinkable SMPs have been used to fabricate surfaces that separate and purify target molecules of interest. Nawaranthna *et al.* used nanoscale magnetic traps formed on the SMP to separate and sort magnetic beads from non-magnetic beads with high purity and throughput.[109] Device fabrication leveraged the surface wrinkling properties of the heat-shrinkable SMP polymer to create multi-scale ferromagnetic Ni structures. The fabricated devices also demonstrated improved efficacy of DNA extraction and purification for quantitative polymerase chain reaction (qPCR) processes relative to the gold standard Qiagen QIAmp DNA Mini Kit (~5.0 ng μL^{-1} and 1.1 ng μL^{-1}, respectively). This technology represents a simple way to separate target species from small sample volumes and is readily amenable towards other operations, such as cell or protein sorting.

Other components (focusing, patterning, energy conversion)—Micro- and nanofabrication using SMP films have resulted in other various device components that include functions such as optical focusing, cell patterning, and energy converting. Dyer *et al.* created plastic microlens arrays by combining photolithography with sequential shrinking processes.[110] An array of dots was printed onto a PS sheet and shrunk. The miniaturized spots were then used as a mask to pattern photoresist onto PO film. The sequential shrinking resulted smooth convex photoresist bumps that experienced a total reduction in size of almost 99% from the original pattern. Molding into PDMS allowed for subsequent embossing of features into optical grade plastics such as cyclic olefin copolymer (COC), to form functional microlens arrays with focal length of ~70 μm.

Freschauf *et al.* used the heat-shrinkable PO film to create structurally modified superhydrophobic surfaces.[111] The rough multi-scale wrinkles, derived from the stiffness mismatch between the bimetallic skin layer and the PO film, resulted in air pockets between the water and surface, decreasing the contact between solid and liquid phases to make

the surface extremely water repelling. These features were transferred into various hard plastics, such as PS, PE, polycarbonate (PC), via embossing, rendering these surfaces superhydrophobic. This technology demonstrates an innovative method for creating surfaces that could be used in various antibacterial applications due to the minimal solid-liquid contact at the surface. Because the resulting superhydrophobicity is derived from purely a structural modification as opposed to chemical modification (which can lead to bacterial resistance, chemical toxicity, and require FDA approval), it can be readily integrated into consumer products.

Zhang *et al.* used the heat-shrinkable PS to develop a low-cost photocathode (Fig. 9).[112] Indium tin oxide (ITO) and platinum (Pt) wrinkles and nanogaps were formed by thermally annealing surface modified PS film. The wrinkles and nanogaps not only enhanced absorption via light trapping and scattering for increased energy conversion efficiency (ECE), but also represented increased Pt catalytic surface area. Zhang *et al.* also leveraged the size reduction properties of the heat-shrinkable film to create high aspect ratio titanium oxide micropillar arrays on the photoanode. By introducing micro- and nanostructures on both the photoanode and cathode of the dye-sensitized solar cell (DSSC), Zhang *et al.* was able to achieve an overall ECE enhancement of 59%. The wrinkled DSSC's improved performance over the flat control also points to the possibility of using the shrink technology for other photovoltaic applications, such as quantum dot and organic solar cells.

4. Conclusions and outlook

Micro- and nanofabrication techniques based off lithography and surface wrinkling using heat-shrinkable SMP materials have been described. These methods progressed in the past several years to yield significant advances such as improved structural resolution and nonplanar and three dimensional fabrication. These advancements significantly expand the ways these technologies can be applied. Existing applications of these fabricated structures have been discussed. The structures have been used to recapitulate native tissue orientation and to simplify cell construct processes, potentially motivating tissue engineering and drug screening accuracy. Structures have also been shown to serve as sensing platforms, achieving improved sensitivity over planar substrates and supporting different readout methods. Other device components including channels, mixers, and sample separation/purification zones, all important LOC systems, have been fabricated using the heat-shrinkable SMP materials.

The wide range of applications of the fabricated micro- and nanostructures illustrates great potential for integration of these structures into complete LOC systems. Simple LOC systems have been devised using the heat-shrinkable SMP.[113–115] While these systems combine microfluidic designs with protein assays, the set-up is simple and the demonstrations proof-of-concepts. Continual efforts are necessary to develop this technology into a complete LOC system.

The pre-stressed thermoplastic film is inexpensive and highly compatible with existing large scale roll-to-roll manufacturing methods. Further work needs to be done to adapt the complicated or relatively expensive surface modification methods (such as metal sputter deposition and optical force printing) for upscalability as successful translation of the

SMP-based techniques into manufacturable practices could highly impact the availability of low-cost LOC devices. Many of the fabrication methods described in this review integrate traditional lithographic methods with the shrink technology. Advantages of using the heat-shrinkable SMP include the ability to substitute lower cost processing methods such as printing and plasma etching to yield features with improved resolution. Cleanroom fabrication can be obviated altogether if features > 60 um are desired. The main benefit of the shrink fabrication approach therefore allows users with varying expertise to rapidly and easily create features with improved resolution, regardless of the fabrication approach chosen.

Challenges to overcome the inherent limitations of the heat-shrinkable SMP film still exist. Features fabricated by the heat-shrinkable SMP film are heterogeneous, with aperiodicity. These hurdles can be overcome with innovative ideas as demonstrated.[48, 69, 71] Furthermore, reproducibility of shrink-induced features has been demonstrated (Nguyen, *et al.* showed that the heat-shrinkable PO had tolerances of ~9%).[47] Features derived on the SMP film are dependent on the factors such as heating conditions applied, polymer extrusion quality, constraints on the polymer film, and precision of the surface modification methods. The ability to generate full studies using structures based of heat-shrinkable SMP films also highlights the reproducibility of resulting technologies.

The applications discussed in this review highlight the unique and versatile properties of the heat-shrinkable SMP-derived structures. While complete LOC systems based off heat-shrinkable SMP films has yet to be realized, existing LOC technologies can gain much by integrating these components. We believe that these structures offer powerful and inexpensive solutions towards existing LOC technologies.

Acknowledgements

This work was supported by the National Institute of Health (NIH) and the National Science Foundation (NSF)'s Integrative Graduate Education and Research Traineeship (IGERT) program in Biophotonics across Energy, Space and Time (BEST).

Notes and references

1. Gates BD, Xu Q, Love JC, Wolfe DB and Whitesides GM, Annu Rev Mater Res, 2004, 34, 339–372.
2. Sharma H, Diep N, Chen A, Lew V and Khine M, Ann Biomed Eng, 2011, 39, 1313–1327. [PubMed: 21152984]
3. Zhao XM, Xia YN and Whitesides GM, J Mater Chem, 1997, 7, 1069–1074.
4. Chen Y and Pepin A, Electrophoresis, 2001, 22, 187–207. [PubMed: 11288885]
5. Gates BD, Xu QB, Stewart M, Ryan D, Willson CG and Whitesides GM, Chem Rev, 2005, 105, 1171–1196. [PubMed: 15826012]
6. Ozin GA, Hou K, Lotsch BV, Cademartiri L, Puzzo DP, Scotognella F, Ghadimi A and Thomson J, Mater Today, 2009, 12, 12–23.
7. Park SM, Liang XG, Harteneck BD, Pick TE, Hiroshiba N, Wu Y, Helms BA and Olynick DL, ACS Nano, 2011, 5, 8523–8531. [PubMed: 21995511]
8. Mather PT, Luo XF and Rousseau IA, Annu Rev Mater Res, 2009, 39, 445–471.
9. Lendlein A, Jiang HY, Junger O and Langer R, Nature, 2005, 434, 879–882. [PubMed: 15829960]
10. Li MH, Keller P, Li B, Wang XG and Brunet M, Adv Mater, 2003, 15, 569–572.

11. Yu YL, Nakano M and Ikeda T, Nature, 2003, 425, 145–145. [PubMed: 12968169]
12. Iqbal D and Samiullah MH, Materials, 2013, 6, 116–142. [PubMed: 28809298]
13. Jiang HY, Kelch S and Lendlein A, Adv Mater, 2006, 18, 1471–1475.
14. Lv HB, Leng JS, Liu YJ and Du SY, Adv Eng Mater, 2008, 10, 592–595.
15. Huang WM, Yang B, An L, Li C and Chan YS, Appl Phys Lett, 2005, 86.
16. Small W, Singhal P, Wilson TS and Maitland DJ, J Mater Chem, 2010, 20, 3356–3366. [PubMed: 21258605]
17. Xie T, Polymer, 2011, 52, 4985–5000.
18. Rousseau IA, Polym Eng Sci, 2008, 48, 2075–2089.
19. Dietsch B and Tong T, J Adv Mater-Covina, 2007, 39, 3–12.
20. Ratna D and Karger-Kocsis J, J Mater Sci, 2008, 43, 254–269.
21. Liu C, Qin H and Mather PT, J Mater Chem, 2007, 17, 1543–1558.
22. Behl M, Razzaq MY and Lendlein A, Adv Mater, 2010, 22, 3388–3410. [PubMed: 20574951]
23. Lendlein A and Kelch S, Angew Chem Int Edit, 2002, 41, 2034–2057.
24. Ota S, Radiat Phys Chem, 1981, 18, 81–87.
25. Nanda S, Rao DVS and Krishnamurthy S, Postharvest Biol Tec, 2001, 22, 61–69.
26. Hsiue GH, Yeh TS and Chang S, J Appl Polym Sci, 1989, 37, 2803–2816.
27. De Francesco A and Duckett RA, Polymer, 2004, 45, 4297–4306.
28. Morshedian J, Khonakdar HA, Mehrabzadeh M and Eslami H, Adv Polym Tech, 2003, 22, 112–119.
29. Richards JRL, Google Patents, 1960.
30. Mueller WB, Google Patents, 1985.
31. Khonakdar HA, Morshedian J, Mehrabzadeh M, Wagenknecht U and Jafari SH, Eur Polym J, 2003, 39, 1729–1734.
32. Hong CK, Maeng H, Song K and Kaang S, J Appl Polym Sci, 2009, 112, 886–895.
33. Chen W, Xing K and Sun L, Radiat Phys Chem, 1983, 22, 593–601.
34. Morshedian J, Khonakdar HA and Rasouli S, Macromol Theor Simul, 2005, 14, 428–434.
35. Fu L, Jiang Z, Enderle H-F, Lilfe D, Li X Funari SS, and Men Y, J Polym Sci Pol Phys, 2013.
36. Shih WK, Polym Eng Sci, 1994, 34, 1121–1128.
37. Datta SK, Chaki TK, Tikku VK, Pradhan NK and Bhowmick AK, Radiat Phys Chem, 1997, 50, 399–405.
38. Mishra JK, Kim I and Ha CS, Macromol Rapid Comm, 2004, 25, 1851–1855.
39. Sharma RR, Pal RK, Singh D, Samuel DVK, Sethi S and Kumar A, J Food Sci Tech Mys, 2013, 50, 590–594.
40. D'Aquino S, Palma A, Schirra M, Continella A, Tribulato E and La Malfa S, Postharvest Biol Tec, 2010, 55, 121–128.
41. Sharma RR, Pal RK and Rana V, Indian J Hortic, 2012, 69, 404–408.
42. Hidber PC, Nealey PF, Helbig W and Whitesides GM, Langmuir, 1996, 12, 5209–5215.
43. Zhao XM, Xia YN, Qin D and Whitesides GM, Adv Mater, 1997, 9, 251–&.
44. Zhao XM, Xia YN, Schueller OJA, Qin D and Whitesides GM, Sensor Actuat a-Phys, 1998, 65, 209–217.
45. Lee AJ, Withford MJ and Dawes JM, Appl Phys a-Mater, 2005, 80, 1447–1449.
46. Zhu XL and Cui TH, Sensor Actuat a-Phys, 2013, 195, 21–26.
47. Nguyen D, Taylor D, Qian K, Norouzi N, Rasmussen J, Botzet S, Lehmann M, Halverson K and Khine M, Lab Chip, 2010, 10, 1623–1626. [PubMed: 20517559]
48. Zhang B, Zhang M and Cui TH, Appl Phys Lett, 2012, 100.
49. Ma T, Liang HS, Chen G, Poon B, Jiang HQ and Yu HB, Opt Express, 2013, 21, 11994–12001. [PubMed: 23736421]
50. Yu CJ, O'Brien K, Zhang YH, Yu HB and Jiang HQ, Appl Phys Lett, 2010, 96.

51. Zhu WJ, Low T, Perebeinos V, Bol AA, Zhu Y, Yan HG, Tersoff J and Avouris P, Nano Lett, 2012, 12, 3431–3436. [PubMed: 22646513]
52. Chan EP, Smith EJ, Hayward RC and Crosby AJ, Adv Mater, 2008, 20, 711–+.
53. Li B, Cao YP, Feng XQ and Gao HJ, Soft Matter, 2012, 8, 5728–5745.
54. Chung JY, Nolte AJ and Stafford CM, Adv Mater, 2011, 23, 349–368. [PubMed: 20814918]
55. Schweikart A and Fery A, Microchim Acta, 2009, 165, 249–263.
56. Bowden N, Brittain S, Evans AG, Hutchinson JW and Whitesides GM, Nature, 1998, 393, 146–149.
57. Efimenko K, Rackaitis M, Manias E, Vaziri A, Mahadevan L and Genzer J, Nat Mater, 2005, 4, 293–297. [PubMed: 15750598]
58. Stafford CM, Harrison C, Beers KL, Karim A, Amis EJ, Vanlandingham MR, Kim HC, Volksen W, Miller RD and Simonyi EE, Nat Mater, 2004, 3, 545–550. [PubMed: 15247909]
59. Regehr KJ, Domenech M, Koepsel JT, Carver KC, Ellison-Zelski SJ, Murphy WL, Schuler LA, Alarid ET and Beebe DJ, Lab Chip, 2009, 9, 2132–2139. [PubMed: 19606288]
60. Toepke MW and Beebe DJ, Lab Chip, 2006, 6, 1484–1486. [PubMed: 17203151]
61. Fu CC, Grimes A, Long M, Ferri CGL, Rich BD, Ghosh S, Ghosh S, Lee LP, Gopinathan A and Khine M, Adv Mater, 2009, 21, 4472–+.
62. Huntington MD, Engel CJ, Hryn AJ and Odom TW, Acs Appl Mater Inter, 2013, 5, 6438–6442.
63. Lin PC and Yang S, Appl Phys Lett, 2007, 90.
64. Yin J, Yague JL, Eggenspieler D, Gleason KK and Boyce MC, Adv Mater, 2012, 24, 5441–5446. [PubMed: 22915065]
65. Zhao Y, Huang WM and Fu YQ, J Micromech Microeng, 2011, 21.
66. Lee MH, Huntington MD, Zhou W, Yang JC and Odom TW, Nano Lett, 2011, 11, 311–315. [PubMed: 20687596]
67. Genzer J and Groenewold J, Soft Matter, 2006, 2, 310–323. [PubMed: 32646128]
68. Chen CS, Breslauer DN, Luna JI, Grimes A, Chin WC, Leeb LP and Khine M, Lab Chip, 2008, 8, 622–624. [PubMed: 18369519]
69. Liu XC, Chakraborty A and Luo C, J Micromech Microeng, 2010, 20.
70. Chakraborty A, Liu XC and Luo C, Sensor Actuat a-*Phys*, 2012, 188, 374–382.
71. Liu Y, Boyles JK, Genzer J and Dickey MD, Soft Matter, 2012, 8, 1764–1769.
72. Kim DH, Lipke EA, Kim P, Cheong R, Thompson S, Delannoy M, Suh KY, Tung L and Levchenko A, P Natl Acad Sci USA, 2010, 107, 565–570.
73. Grosberg A, Alford PW, McCain ML and Parker KK, Lab Chip, 2011, 11, 4165–4173. [PubMed: 22072288]
74. Luna JI, Ciriza J, Garcia-Ojeda ME, Kong M, Herren A, Lieu DK, Li RA, Fowlkes CC, Khine M and McCloskey KE, Tissue Eng Part C-Me, 2011, 17, 579–588.
75. Chen A, Lieu DK, Freschauf L, Lew V, Sharma H, Wang JX, Nguyen D, Karakikes I, Hajjar RJ, Gopinathan A, Botvinick E, Fowlkes CC, Li RA and Khine M, Adv Mater, 2011, 23, 5785–+. [PubMed: 22065428]
76. Bursac N, Parker KK, Iravanian S and Tung L, Circ Res, 2002, 91, E45–E54. [PubMed: 12480825]
77. Au HTH, Cheng I, Chowdhury MF and Radisic M, Biomaterials, 2007, 28, 4277–4293. [PubMed: 17604100]
78. Yang F, Murugan R, Wang S and Ramakrishna S, Biomaterials, 2005, 26, 2603–2610. [PubMed: 15585263]
79. Chew SY, Mi R, Hoke A and Leong KW, Biomaterials, 2008, 29, 653–661. [PubMed: 17983651]
80. Whited BM and Rylander MN, Biotechnol Bioeng, 2014, 111, 184–195. [PubMed: 23842728]
81. Dalby MJ, Riehle MO, Sutherland DS, Agheli H and Curtis AS, Eur Cell Mater, 2005, 9, 1–8; discussion 8. [PubMed: 15690263]
82. Wang JX, Chen A, Lieu DK, Karakikes I, Chen GP, Keung WD, Chan CW, Hajjar RJ, Costa KD, Khine M and Li RA, Biomaterials, 2013, 34, 8878–8886. [PubMed: 23942210]
83. Turner WS, Wang XL, Johnson S, Medberry C, Mendez J, Badylak SF, McCord MG and McCloskey KE, J Biomed Mater Res B, 2012, 100B, 2060–2072.

84. Chen A, Lee E, Tu R, Santiago K, Grosberg A, Fowlkes C and Khine M, Biomaterials, 2014, 35, 675–683. [PubMed: 24144905]
85. Hatano R, Mercurio K, Luna JI, Glaser DE, Leppert VJ and McCloskey KE, J Biol Eng, 2013, 7, 18. [PubMed: 23819656]
86. Greco F, Fujie T, Ricotti L, Taccola S, Mazzolai B and Mattoli V, Acs Appl Mater Inter, 2013, 5, 573–584.
87. Kurosawa H, J Biosci Bioeng, 2007, 103, 389–398. [PubMed: 17609152]
88. Chen CS, Pegan J, Luna J, Xia B, McCloskey K, Chin WC and Khine M, J Vis Exp, 2008.
89. Grimes A, Breslauer DN, Long M, Pegan J, Lee LP and Khine M, Lab Chip, 2008, 8, 170–172. [PubMed: 18094775]
90. Nguyen D, Sa S, Pegan JD, Rich B, Xiang GX, McCloskey KE, Manilay JO and Khine M, Lab Chip, 2009, 9, 3338–3344. [PubMed: 19904398]
91. Lew V, Nguyen D and Khine M, Jala-J Lab Autom, 2011, 16, 450–456.
92. Le Goff GC, Blum LJ and Marquette CA, Macromol Biosci, 2013, 13, 227–233. [PubMed: 23335561]
93. Pegan JD, Ho AY, Bachman M and Khine M, Lab Chip, 2013, 13, 4205–4209. [PubMed: 24056907]
94. Lin S, Sharma H and Khine M, Adv Opt Mater, 2013, 1, 568–572.
95. Greco F, Ventrelli L, Dario P, Mazzolai B and Mattoli V, Int J Hydrogen Energ, 2012, 37, 17529–17539.
96. Zhang B and Cui TH, J Microelectromech S, 2013, 22, 1140–1146.
97. Ross BM, Wu LY and Lee LP, Nano Lett, 2011, 11, 2590–2595. [PubMed: 21661733]
98. Urban AS, Fedoruk M, Nedev S, Lutich A, Lohmueller T and Feldmann J, Adv Opt Mater, 2013, 1, 123–127.
99. Fu CC, Ossato G, Long M, Digman MA, Gopinathan A, Lee LP, Gratton E and Khine M, Appl Phys Lett, 2010, 97.
100. Sharma H, Digman MA, Felsinger N, Gratton E and Khine M, Opt Mater Express, 2014, 4, 753–763. [PubMed: 25383253]
101. Zhang L, Lang XY, Hirata A and Chen MW, ACS Nano, 2011, 5, 4407–4413. [PubMed: 21627303]
102. Liu HW, Zhang L, Lang XY, Yamaguchi Y, Iwasaki HS, Inouye YS, Xue QK and Chen MW, Sci Rep-Uk, 2011, 1.
103. Taylor D, Dyer D, Lew V and Khine M, Lab Chip, 2010, 10, 2472–2475. [PubMed: 20680207]
104. Swaminathan S and Cui Y, Rsc Adv, 2012, 2, 12724–12727.
105. Chakraborty A, Xiang MM and Luo C, Materials, 2013, 6, 3610–3623. [PubMed: 28811456]
106. Liu RH, Yang JN, Pindera MZ, Athavale M and Grodzinski P, Lab Chip, 2002, 2, 151–157. [PubMed: 15100826]
107. Long M, Sprague MA, Grimes AA, Rich BD and Khine M, Appl Phys Lett, 2009, 94.
108. Jayadev S, Pegan J, Dyer D, McLane J, Lim J and Khine M, Smart Mater Struct, 2013, 22.
109. Nawarathna D, Norouzi N, McLane J, Sharma H, Sharac N, Grant T, Chen A, Strayer S, Ragan R and Khine M, Appl Phys Lett, 2013, 102.
110. Dyer D, Shreim S, Jayadev S, Lew V, Botvinick E and Khine M, Appl Phys Lett, 2011, 99.
111. Freschauf LR, McLane J, Sharma H and Khine M, Plos One, 2012, 7.
112. Zhang B, Zhang M, Song KP, Li Q and Cui TH, Appl Phys Lett, 2013, 103.
113. Sollier K, Mandon CA, Heyries KA, Blum LJ and Marquette CA, Lab Chip, 2009, 9, 3489–3494. [PubMed: 20024027]
114. Mandon CA, Heyries KA, Blum LJ and Marquette CA, Biosens Bioelectron, 2010, 26, 1218–1224. [PubMed: 20541390]
115. Nguyen D, McLane J, Lew V, Pegan J and Khine M, Biomicrofluidics, 2011, 5.

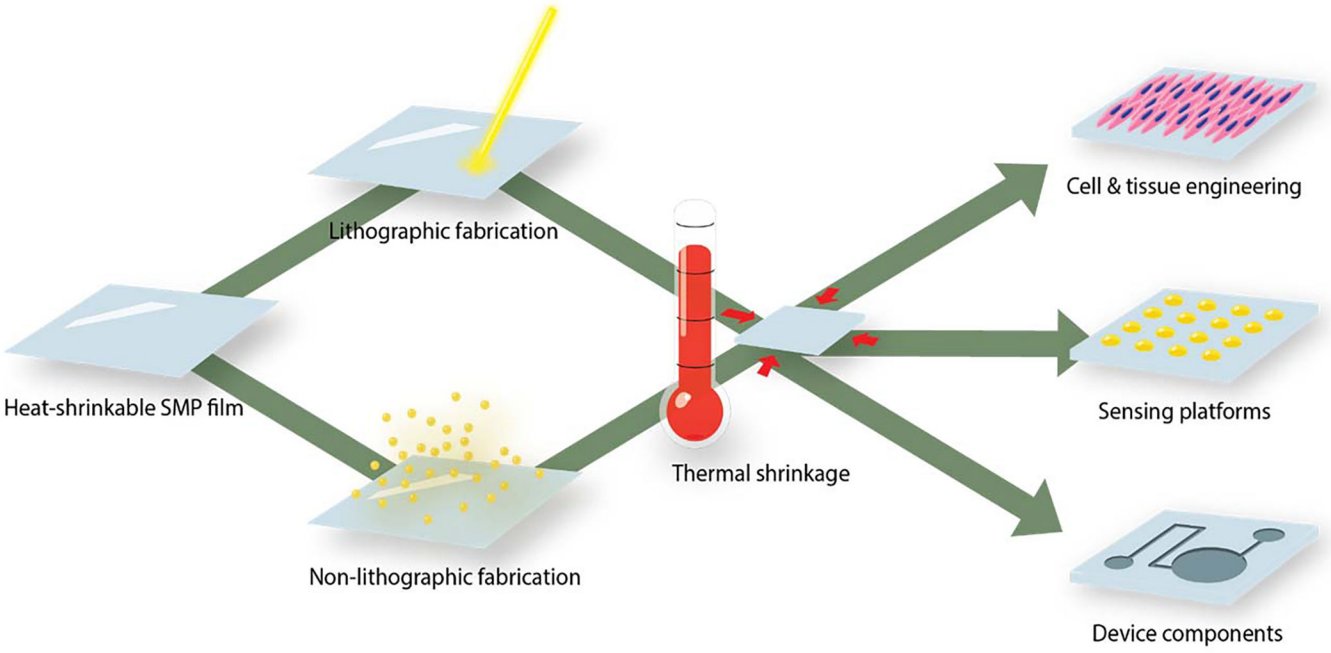

Fig 1.

Schematic illustrating techniques for micro- and nanofabrication using the heat-shrinkable SMP film and current existing applications of the resulting features covered in this review.

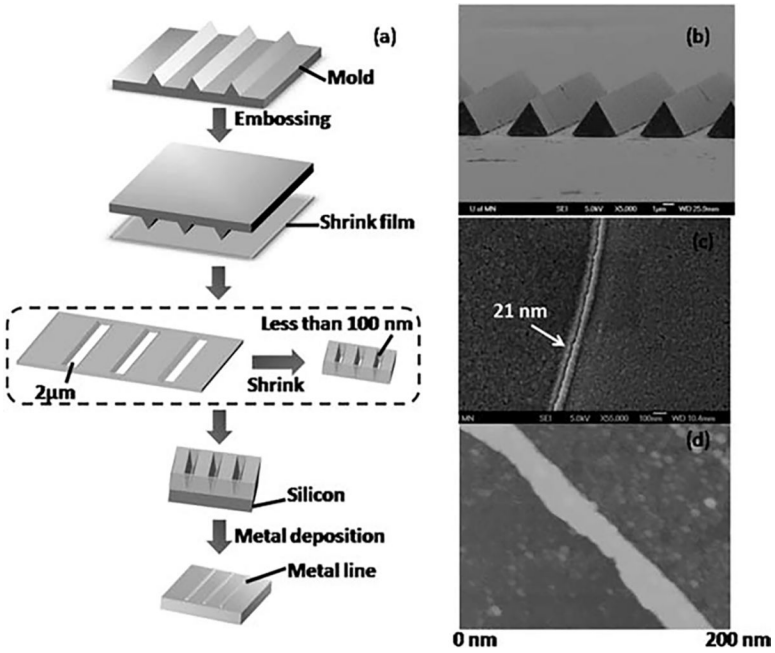

Fig 2.

a) Incorporation of hot-embossing techniques with shrink technology results in reduced feature sizes. SEM images of b) the metal mold and c) the 21 nm line. d) AFM image of the 21 nm line. Adapted from B. Zhang, M. Zhang and T. H. Cui, *Appl Phys Lett*, 2012, 100 with permission from AIP Publishing. [47]

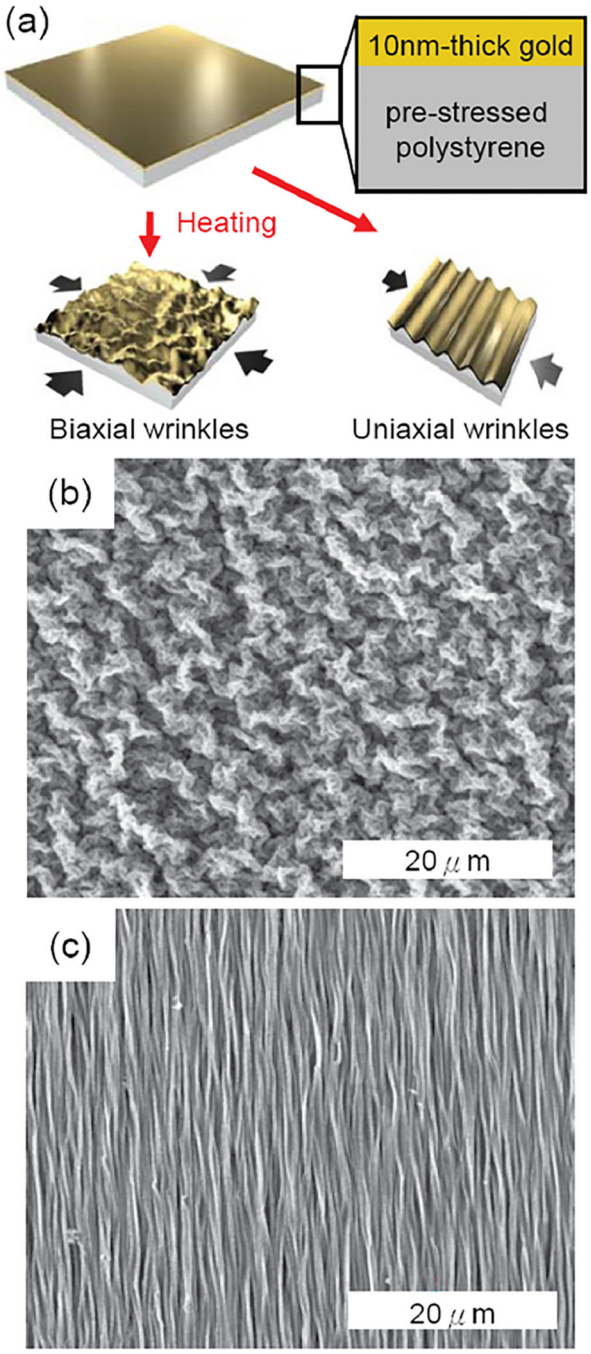

Fig 3.

Micro- and nanofabrication on heat-shrinkable SMP film via surface wrinkling.[60] a) Scheme of fabrication of biaxial (left) and uniaxial (right) wrinkles on polystyrene sheets. SEM images of resulting b) biaxial and c) uniaxial wrinkles using gold. Adapted from C. C. Fu, A. Grimes, M. Long, C. G. L. Ferri, B. D. Rich, S. Ghosh, S. Ghosh, L. P. Lee, A. Gopinathan and M. Khine, *Adv Mater*, 2009, 21, 4472-+ with permission from John Wiley and Sons.

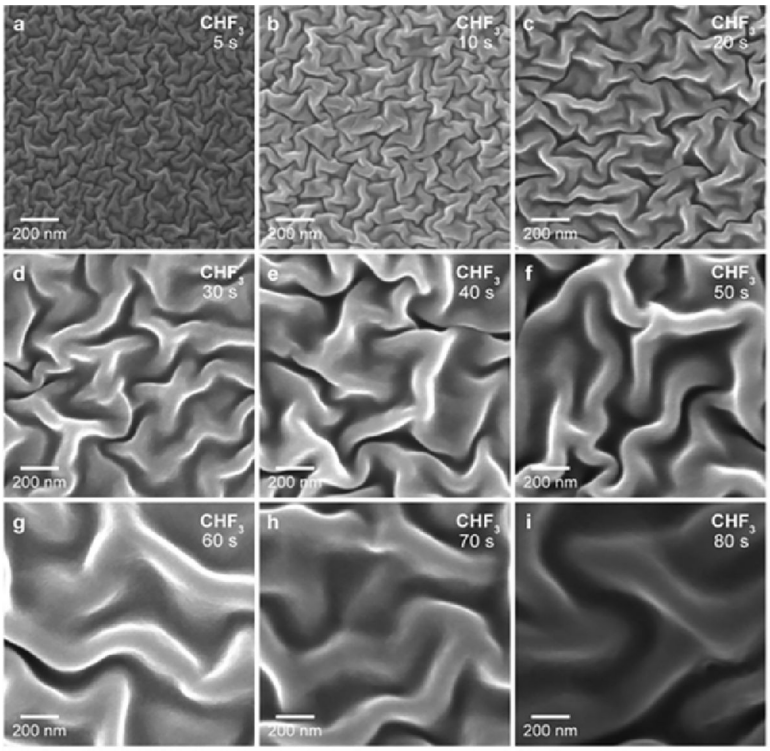

Fig 4.

Characteristic wavelengths of PS films tuned by changing the RIE exposure time.[61] SEM images of 2D nanowrinkles formed by RIE with CHF_3 and times of a) 5 s (λ = 34 nm), b) 10 s (λ = 44 nm), c) 20 s (λ = 107 nm), d) 30 s (λ = 162 nm), e) 40 s (λ = 198 nm), f) 50 s (λ = 228 nm), g) 60 s (λ = 303 nm), h) 70 s (λ = 360 nm), and i) 80 s (λ = 431 nm). Adapted with permission from M. D. Huntington, C. J. Engel, A. J. Hryn and T. W. Odom, *Acs Appl Mater Inter*, 2013, 5, 6438–6442. Copyright 2013 American Chemical Society.

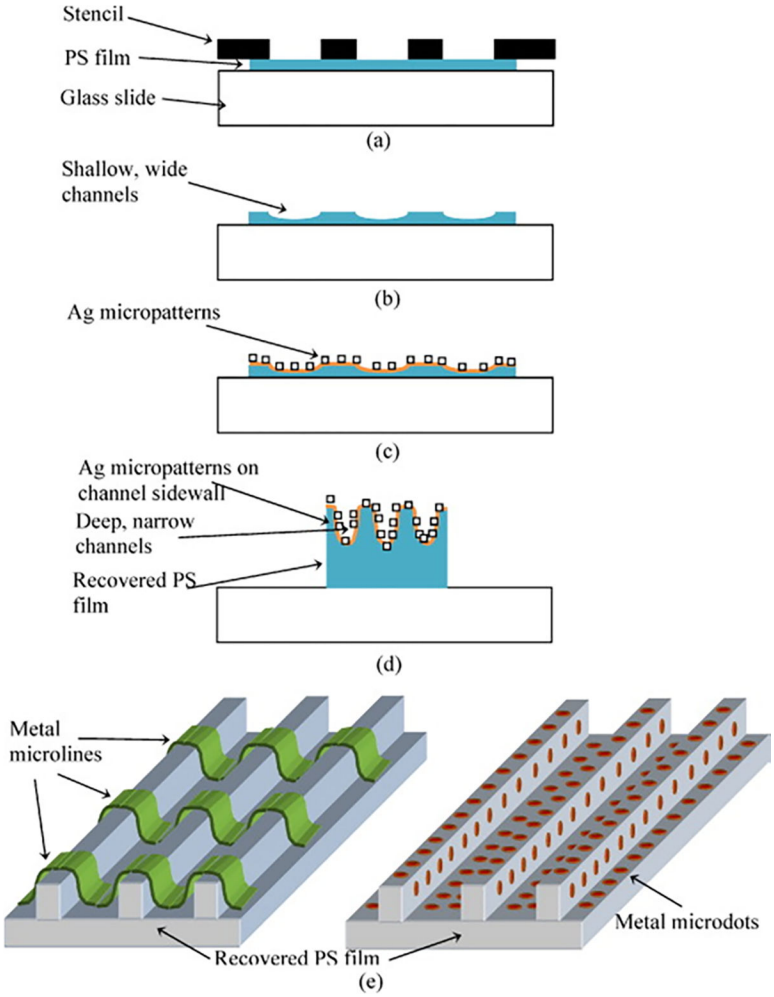

Fig 5.

Schematic showing the fabrication procedure of PS channels containing sidewall and bottom patterns.[69] a) shallow, wide channels are etched inside the PS film using a mask; b) removal of the mask reveals channels; c) Ag micropatterns are produced on the substrate using another mask; and d) after strain recovery of the PS block, the Ag micropatterns are transferred to the channel sidewalls. e) 3D visualizations of resulting PS channels covered with Ag microlines and microdots. Adapted from A. Chakraborty, X. C. Liu and C. Luo, *Sensor Actuat a-Phys*, 2012, 188, 374–382 with permission from Elselvier.

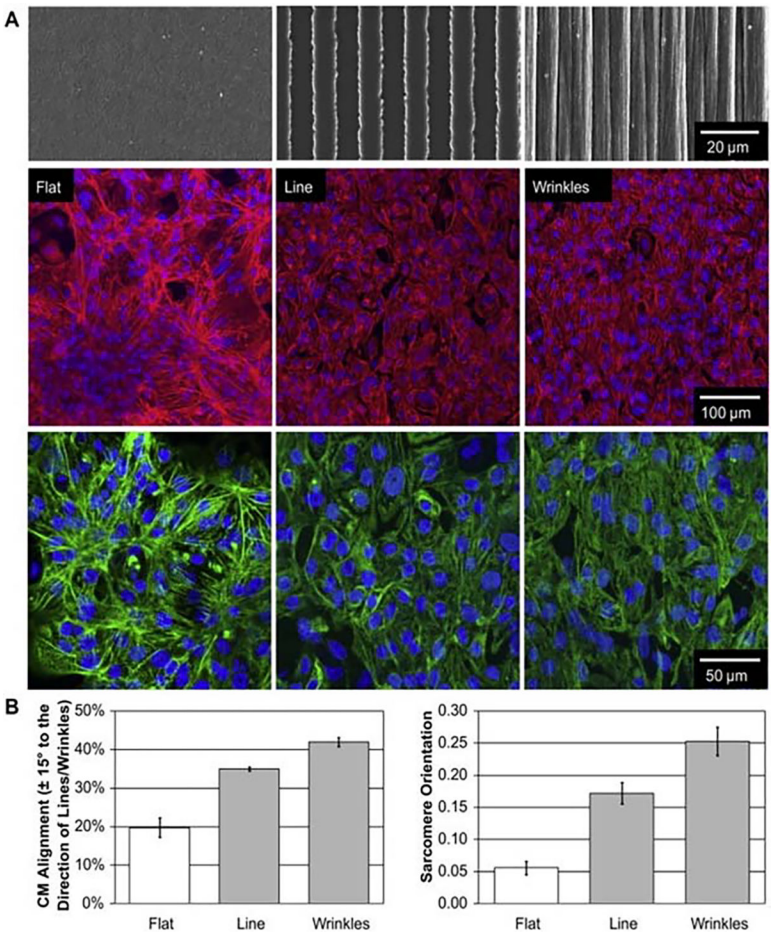

Fig 6.

Comparing alignment of hESC-CMs on control surfaces to the wrinkle patterned substrates.[83] a) SEM images of the three types of substrates at 1000x magnification (top panel). Fluorescent images of f-actin (red) in hESC-CMs seeded on the various topographies. Nuclei of hESC-CMs were stained with DAPI (blue) (middle panel). Fluorescent images of α-actinin (green) in hESC-CMs seeded on the various topographies. Nuclei of hESC-CMs were stained with DAPI (blue) (bottom panel). b) Percentage of f-actin aligned to the direction of the line/wrinkles (left panel). Measurement of sarcomere alignment efficiency using the orientation organization parameter (right panel). Adapted from A. Chen, E. Lee, R. Tu, K. Santiago, A. Grosberg, C. Fowlkes and M. Khine, *Biomaterials*, 2014, **35**, 675–683 with permission from Elselvier.

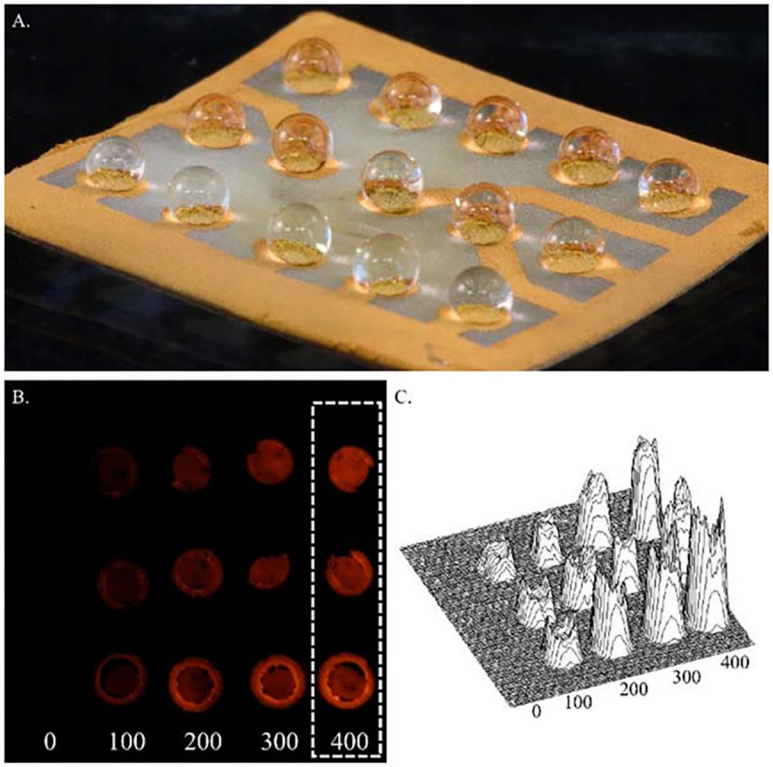

Fig. 7.

Shrunk ECL sensor with optical read out methods.[92] a) Wrinkled Au thin film electrodes with samples on patterned detection zones. b) Luminescent images from the CMOS sensor. c) 3D intensity profile of detection zones. Adapted from J. D. Pegan, A. Y. Ho, M. Bachman and M. Khine, *Lab Chip*, 2013, 13, 4205–4209 with permission from the Royal Society of Chemistry.

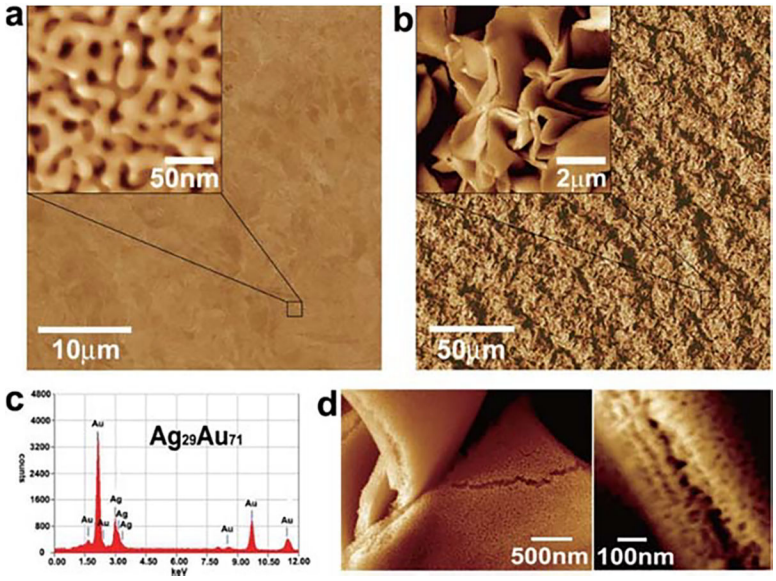

Fig. 8.

Shrinkage of nanoporous thin films result in nanostructures for SERS effects.[101] SEM images of a) flat nanoporous films and b) features arising from shrinking nanoporous thin films. c) Chemical composition of the thin films. d) SEM image showing nanogaps hot spots for SERS effects. Adapted from H. W. Liu, L. Zhang, X. Y. Lang, Y. Yamaguchi, H. S. Iwasaki, Y. S. Inouye, Q. K. Xue and M. W. Chen, *Sci Rep*-Uk, 2011, 1 with permission from Nature Publishing Group.

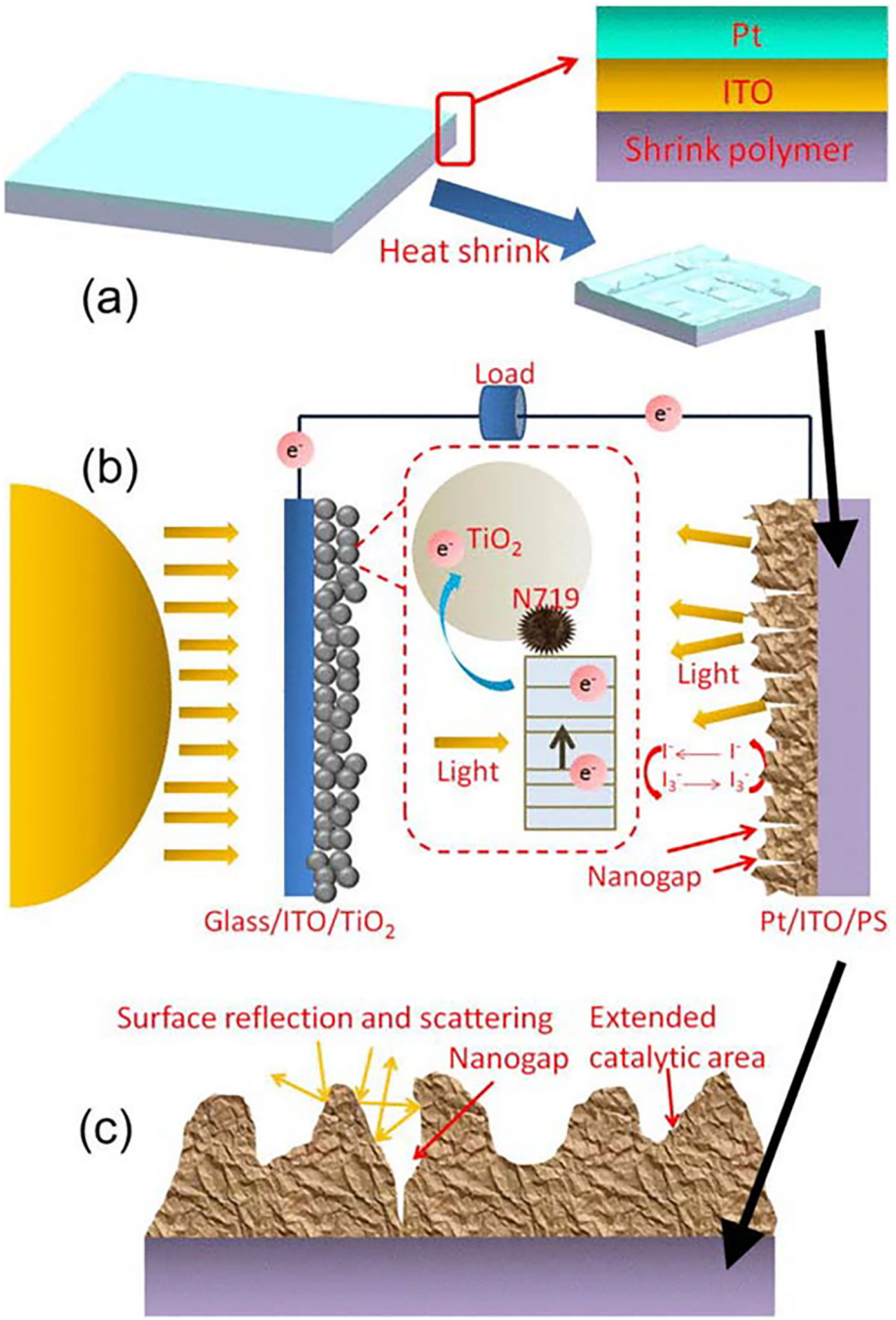

Fig 9.

Schematic diagram of DSSCs with shrink induced wrinkles and nanogaps on the photocathodes.[111] a) Fabrication process of shrink-induced wrinkles and nanogaps. The shrink polymer substrate with wrinkles and nanogaps generated on the top surface serves as the photocathode. b) DSSC incorporation with shrink-induced structures. c) Shrink-induced wrinkles and nanogaps on photocathodes enhance the incident light scattering and Pt

catalytic area. Adapted from B. Zhang, M. Zhang, K. P. Song, Q. Li and T. H. Cui, *Appl Phys Lett*, 2013, 103 with permission from AIP Publishing.